

On the Density profile slope of Clusters of Galaxies

A. Del Popolo^{1,2*}

¹*Dipartimento di Fisica e Astronomia, Università di Catania, Viale Andrea Doria 6, 95125 Catania, Italy*

²*Departamento de Astronomia, Universidade de São Paulo, Rua do Matão 1226, 05508-900, São Paulo, SP, Brazil*

18 October 2018

ABSTRACT

The present paper extends to clusters of galaxies the study of Del Popolo (2012), concerning how the baryon-dark matter (DM) interplay shapes the density profile of dwarf galaxies. Cluster density profiles are determined taking into account dynamical friction, random and ordered angular momentum and the response of dark matter halos to condensation of baryons. We find that halos containing only DM are characterized by Einasto’s profiles, and that the profile flattens with increasing content of baryons, and increasing values of random angular momentum. The analytical results obtained in the first part of the paper were applied to well studied clusters whose inner profiles have slopes flatter than NFW predictions (A611, A383) or are characterized by profiles in agreement with the NFW model (MACS J1423.8+2404, RXJ1133). By using independently-measured baryonic fraction, a typical spin parameter value $\lambda \simeq 0.03$, and adjusting the random angular momentum, we re-obtain the mass and density profiles of the quoted clusters. Finally, we show that the baryonic mass inside $\simeq 10$ kpc, $M_{b,in}$ is correlated with the total mass of the clusters, as $M_{b,in} \propto M_{500}^{0.4}$.

Key words: cosmology–theory–large scale structure of Universe–galaxies–formation

1 INTRODUCTION

The Λ CDM model is remarkably successful in fitting a wide range of data of large-scale structures, starting from the anisotropy and polarization spectrum of cosmic microwave background radiation (Spergel et al. 2003; Komatsu et al. 2011), passing through the high-redshift studies of the Ly α forest, and going on with the Hubble diagram of Type Ia Supernovae (Kowalski et al 2008), and the matter power spectrum with its Baryonic Acoustic Oscillation features (Percival et al. 2010).

In spite of the success of Λ CDM predictions on cosmological scales, the model has shown difficulties in giving correct predictions on galaxy scales, especially for what concerns the central density expected in dark matter haloes. Dwarfs and low surface brightness (LSB) galaxies, objects that are dark matter dominated, are characterized by kinematics, and rotation curves, incompatible with haloes predicted by Λ CDM, as obtained in dissipationless N-body simulations (Navarro et al. 1996, 1997, hereafter NFW; Moore et al. 1998; Jing & Suto 2000, Klypin et al. 2001; Hayashi et al. 2004; Power et al. 2003; Navarro et al. 2004, 2010).

While dissipationless N-body simulations predict cuspy profiles¹, observations show that the inner part of density profiles is characterized by a core-like structure (e.g., Flores & Primak 1994; Moore 1994; Kravtsov et al. 1998; de Blok & Bosma 2002; de Blok, Bosma & McGaugh 2003; Gentile et al. 2004, 2006; Blaise-Ouelette et al. 2004, Spanó et al. 2008, Kuzio de Naray et al. 2008, 2009, and Oh et al. 2010). The quoted discrepancy between observations and simulations is known as the Cusp-Core problem².

Another important test of the results of numerical simulations is to check their predictions also on cluster scales. Constraints on DM density profiles are more straightforward to obtain in clusters of galaxies than in galaxies,³ since clusters have several measurable properties that can be understood and interpreted in a simpler fashion

¹ The inner density profile predicted by simulations is characterized by $\rho \propto r^{-1}$ for the NFW model, $\rho \propto r^{-1.5}$ in the Moore et al. (1998) model, and by the Einasto profile, shallowing towards the center of the halo, in more recent simulations (e.g., Navarro et al. 2010). Stadel et al. (2009) found $\alpha \simeq 0.8$ at 120 pc.

² For the sake of precision, we have to report that some observations found density profiles compatible with both cuspy and cored profiles (van den Bosch et al. 2000; Swaters et al. 2003a,b; Spekkens et al. 2005; Simon et al. 2005; de Blok et al. 2008).

³ Even if a drawback in using clusters is that the mass distribu-

* E-mail: antonino.delpopolo@unibg.it

than galaxies rotation curves. For example, X-ray emission from the intracluster plasma at radii of the order of 10% of the virial radius (r_{vir}) can easily be observed and the gas temperature profile can be measured with observations (e.g., with Chandra or XMM).

Nevertheless many studies have used X-ray observations of the hot intracluster medium, under the assumption of hydrostatic equilibrium, X-ray data alone have difficulties in constraining the mass distribution, especially in the central regions. This is because even relaxed clusters tend to have “cooling flows”. In these clusters X-ray emission is often disturbed and the assumption of hydrostatic equilibrium is questionable (see Arabadjis, Bautz & Arabadjis 2004).

X-ray temperature measurements are carried out from 500 kpc (Bradáč et al. 2008) to $\simeq 50$ kpc, and the determination of temperature at smaller radii are limited by instrumental resolution or substructure (Schmidt & Allen 2007). X-ray analyses have obtained wide ranging values of the inner slope, α , of the density profile with α ranging from $\simeq 0.6$ (Ettori et al. 2002) through $\simeq 1.2$ (Lewis, Buote & Stocke 2003) to $\simeq 1.9$ (Arabadjis, Bautz & Garmire 2002), while *Chandra* and *XMM-Newton* results suggest good agreement with CDM predictions (see Schmidt & Allen 2007, and references therein). The value of α obtained by using X-ray observations have the drawback that it is complicated to take account of the stellar mass contained in the brightest cluster galaxy (BCG), located in the cluster center. The central mass, constituted by stars and gas, even if it is small, compared to the total mass of the system, usually dominates the mass at small radii ($\simeq 10$ kpc), with strong implications on the shape of the inner DM profile.

The dark matter distribution in clusters can be also studied through gravitational lensing. Weak lensing of background galaxies is used to reconstruct the mass distribution in the outer parts of clusters (Mellier 1999). This technique is based on averaging noisy signal coming from many background galaxies. The resolution that can be achieved is able to constrain profiles inside ~ 100 kpc. An example of its application was given by Dahle, Hannestad & Sommer-Larsen (2003), who found that the average profile of 6 clusters agrees with the NFW profile at radii $r \geq 0.1r_{vir}$, even though with large uncertainties.

In the central parts of the cluster, lensing effects become non-linear and one can use the strong lensing technique, in order to constrain the mass distribution. This technique has a typical sensitivity to the projected mass distribution inside ~ 100 – 200 kpc, with limits at ~ 10 – 20 kpc (Gavazzi 2005; Limousin et al. 2008). Typical structures observed in the strong lensing regime are radial arcs, located in positions corresponding to the local derivative of the cluster mass density profile, and tangential arcs whose position is determined by the projected mass density interior to the arc.

tion in clusters is usually affected by the growth of the central galaxy.

Example of application of the lensing method are Smith et al. (2001), who studied the tangential and radial arcs of A383, finding an inner slope of the total mass density profile $\alpha > 1$ at a radius $\sim 1\%r_{vir}$. Sand et al. (2004), and Newman et al. (2011), after removing the baryonic component, with the aid of stellar kinematics, found that the dark matter only inner slope is flatter than 1. Kneib et al. (2003) studied Cl 0024+1654 by means of strong and weak lensing finding that a NFW profile fits the profile from $0.1r_{vir}$ to several values of r_{vir} (but Tyson, Kochansky & Dell’Antonio 1998 found $\alpha = 0.57 \pm 0.024$). Gavazzi et al. (2003), and Gavazzi (2005) studied MS2137.3-2353 concluding that the precise value of the slope depends on the mass-to-light ratio of the BCG (but Sand et al. 2002, found a cored profile with $\alpha \simeq 0.35$).

As it is clear from the previous examples, strong gravitational lensing has given controversial results, and in several cases α values are much smaller than Λ CDM predictions. Moreover, similarly to X-ray analyses, lensing alone cannot disentangle the DM and baryonic components. Better constraints on the central part of the density profiles can be obtained through stellar kinematics of the central galaxy (~ 1 – 200 kpc region), and even better results are obtained combining all the previous methods (Miralda-Escude 1995; Kneib et al. 2003, (weak+strong lensing); Bradač et al. 2005 (weak+strong lensing); Mahdavi et al. 2007 (X-ray+weak lensing)).

As previously reported, distinct researchers, using different techniques, found results going from good agreement with the Λ CDM model to disagreement with it, and what is worse is that this often happened for the very same clusters (Smith et al. 2005; Gavazzi et al. 2005; Zappacosta et al. 2006; Schmidt & Allen 2007; Umetsu & Broadhurst 2008; Bradač et al. 2008; Limousin et al. 2008).

The quoted discrepancies in observational results are probably connected to several factors: a) use of observational techniques with different/limited dynamic range in radius; b) different definition of the slope, which sometime refers to the DM and sometime to the total mass. We should also not forget the scatter in the profile from cluster to cluster, also observed in the case of dwarfs by Simon et al. (2005), which contributes to the quoted discrepancy between observational results; c) not taking into account the stellar mass of the BCG, which is correct for the outer part of the cluster but wrong for the inner part, where stars dominate the density profile. Concerning this last issue, if the baryon-DM interaction changes the density profile, the usual parameterization of the density profile with NFW or generalized Navarro-Frenk-White (gNFW) models, may be inappropriate (Sand et al. 2008). Another important factor that can produce errors is originated if the clusters shape is not taken correctly into account (Gavazzi 2005).

A series of papers by Sand (Sand et al. 2002, 2004, 2008, hereafter S02, S04, and S08), further fed the debate on the shape of DM halos of clusters, and the inner slope of the density profiles. In the quoted papers, Sand combined gravitational lensing with the velocity dispersion profile of the BCG. In this way the author was able to separate the

contribution to the halo coming from the DM from that coming from the stellar mass of the BCG.

S02 studied MS 2137-23 finding a flat inner slope with $\alpha < 0.9$ at 99% CL, and in their best fit parameters, α was 0.35.

S04 studied a sample of 6 clusters (MS 2137-23; A383; A963; RXJ1133; MACS 1206; A1201), three having just tangential arcs, and three also having radial arcs. Combining lensing and velocity dispersion profile of the central galaxy in each case, they found a mean DM distribution inconsistent with the NFW value, $\alpha = 1$ at $> 99\%$ CL. The system of clusters containing radial arcs gives a value of $\alpha = 0.52_{-0.05}^{+0.05}$ (68% CL), and $\alpha < 0.57$ at 99% CL, for the case of the tangential arc sample. If their results are correct, they disagree with Λ CDM model on small scales, unless some physical mechanism not taken into account could get the Λ CDM out of the trouble (e.g., a form of interplay between DM and baryons). Bartelmann & Meneghetti (2004) and Meneghetti et al. (2007) concluded that the flat slopes obtained by Sand were due to an oversimplified assumptions in the analysis, such as negligible ellipticity.

An improved analysis of A383 and MS2137-23, presented by S08, found a flat value for the slope of A383 ($\alpha = 0.45_{-0.2}^{+0.2}$). Newmann et al. (2009) (hereafter N09), presented a detailed analysis of DM and baryonic distribution in A611, combining weak lensing, strong lensing and stellar velocity dispersion for the BCG, finding a slope $\alpha < 0.3$ (68% CL) and similarly, Newman et al. (2011) (hereafter N11) found $\alpha < 1$ (95% CL) for A383. They showed that degeneracies in constraining the DM profile can be broken only simultaneously using the three techniques. The quoted results show that at least some clusters of galaxies have inner density profile slopes shallower that those obtained in N-body simulations.

These results are in agreement with studies on dwarf galaxies, showing that not all dwarfs have core-like rotation curves and that their density profiles are compatible with both cuspy and core profiles (Hayashi et al. 2004; van den Bosch et al. 2000; Swaters et al. 2003a,b; Simon et al. 2005; Spekkens, Giovanelli & Haynes 2005; de Blok et al. 2008). Very interesting is the case studied by Simon et al. (2003, 2005) who found that in a sample of dwarf galaxies, namely NGC 2976, NGC 4605, NGC 5949, NGC 5963, and NGC 6689, the inner slopes goe from very flat to cuspy, more precisely $\alpha = (0.01; 0.78; 0.88; 1.20; 0.79)$, respectively, with a mean slope $\alpha \simeq 0.73$, and a dispersion of 0.44.

de Blok et al. (2008), using a sample from the HI nearby galaxy survey (THINGS) found that the best fit to rotation curves depends on their mass: for galaxies having $M_B < -19$ the NFW profile or the pseudo-isothermal profile statistically fitted equally well, while this what not the case galaxies with $M_B > -19$ the core-dominated pseudo-isothermal model fitted significantly better than the NFW model.

In several previous papers, we studied the role of baryons on the previously quoted problem (e.g., DP09, DP12).

In the present paper, we extend the analysis of DP12

from dwarf galaxies to clusters of galaxies, studying the effects of baryons on the inner DM density profile. Similarly to DP12, the present paper has two aims. The first is to study the role of baryons and random angular momentum in changing clusters of galaxies density profiles. The second is to apply the results of this study to observed clusters, to understand if the model can re-obtain the density profile of some well studied clusters with cuspy, cored and intermediate density profiles.

This paper is organized as follows. Section 2 summarizes the model used. In Section 3.1, we find how changes in baryonic fraction and angular momentum, influence the density profiles. In Section 3.2, we compare the results of Section 3.1 with four different clusters of galaxies. Section 4 is devoted to discussions and Section 5 to conclusions.

2 SUMMARY OF THE MODEL

The density profiles of clusters are obtained using the model discussed in DP09, and DP12. For convenience of the reader, the model is summarized in the following of this section.

DP09 is an improvement of previous spherical infall models (SIM) presented in literature (Gunn & Gott 1972; Fillmore & Goldreich 1984; Bertschinger 1985; Hoffman & Shaham 1985; Ryden & Gunn 1987; Avila-Reese, Firmani & Hernandez 1998; Subramanian et al. 2000; Ascasibar, Yepes & Götteleber 2004; Williams, Babul & Dalcanton 2004).

Differently from previous SIMs, DP09 includes in the model the joint effects of ordered and random angular momentum, dynamical friction, adiabatic contraction of dark matter. Previous SIMs usually took account one effect at a time: random angular momentum (e.g., Williams, Babul & Dalcanton 2004), dynamical friction of stellar/DM clumps against the background halo (e.g., El-Zant et al. 2001; Romano-Diaz et al. 2008), or just adiabatic contraction (e.g., Blumenthal et al. 1986; Gnedin et al. 2004; Klypin, Zhao, and Somerville 2002; Gustafsson et al. 2006).

The main features of the SIM are described by Gunn & Gott (1972). The quoted model assumes that a protostructure is divided into mass shells, each one expanding with the Hubble flow from an initial comoving radius x_i to a maximum one x_m (usually named turn-around radius x_{ta}), and then collapse. Non-linear processes convert the kinetic energy of collapse into random motions, giving rise to a “virialized” structure. The density profile at turn-around, $\rho_{ta}(x_m)$, is obtained following the dynamics of collapse of the shells, assuming that mass is conserved and that each shell is kept at its turn-around radius (Peebles 1980; Hoffman & Shaham 1985; White & Zaritsky 1992).

In order to go on from turn-around to the final collapse, and to obtain the final density profile, one usually assumes that the potential well near the center varies adiabatically (Gunn 1977, Fillmore & Goldreich 1984). The final density is given by

$$\rho(x) = \frac{\rho_{ta}(x_m)}{f^3} \left[1 + \frac{d \ln f}{d \ln x_m} \right]^{-1} \quad (1)$$

where $f = x/x_m$ is the collapse factor (see Eq. A18, DP09). During expansion, the tidal fields originated by the large-scale structure exert a torque on the proto-structure imparting angular momentum on the proto-halo (Hoyle 1953; Peebles 1969; White 1984; Ryden 1988; Eisenstein & Loeb 1995; Catelan & Theuns 1996). After that the proto-structure decouples from the background, turns-around and collapses, tidal torque is noteworthy reduced, since the lever arm is reduced drastically by collapse (Schaefer 2009). Angular momentum originated by tidal torques is calculated obtaining the rms torque, $\tau(r)$, on a mass shell and then calculating the total specific angular momentum, $h(r, \nu)$, acquired during expansion by integrating the torque over time (Ryden 1988, Eq. 35). As shown in DP09, the values obtained for angular momentum are in agreement with others studies (e.g. Catelan & Theuns 1996). As in DP12, total angular momentum is expressed in terms of the dimensionless spin parameter

$$\lambda = \frac{L|E|^{1/2}}{GM^{5/2}}, \quad (2)$$

where L is the angular momentum, summed over shells, and E is the binding energy of the halo. According to Padmannabhan (1993), λ can be interpreted as the ratio of the angular velocity, ω of the system to that, ω_{sup} of the system providing the rotational support, obtaining

$$\lambda = \frac{\omega}{\omega_{sup}} = \frac{L}{2G^{1/2}M^{3/2}R^{1/2}}, \quad (3)$$

In a system constituted by DM and baryons as ours, we have a spin parameter for DM and another for gas

$$\lambda_{gas(DM)} = \frac{L_{gas(DM)}}{M_{gas(DM)}[2G(M_{gas} + M_{DM})r_{vir}^{1/2}]}, \quad (4)$$

where $L_{gas(DM)}$ is the angular momentum of gas(DM), and $M_{gas(DM)}$ the gas(DM) mass inside the virial radius r_{vir} . The ratio of $\lambda_{gas}/\lambda_{DM}$ is fixed according to Götteleber & Yepes (2007) (1.23 for haloes with $M_{vir} > 5 \times 10^{14} h^{-1} M_\odot$ (see their figure 5)). The distribution of the λ parameter is well described by a lognormal distribution (e.g. Vivitska et al. 2002). Götteleber & Yepes (2007) studied the spin parameter of 10,000 clusters extracted from the *Mare Nostrum Universe* SPH simulation, finding a log-normal distribution with best fit parameters given by λ with $\lambda = 0.0351 \pm 0.0016$, $\sigma_\lambda = 0.6470 \pm 0.0067$ for the DM distribution and $\lambda = 0.0462 \pm 0.0012$, $\sigma_\lambda = 0.6086 \pm 0.0030$ for the gas distribution, with $\lambda_{max} = 0.0231, 0.0319$ for DM and gas distributions (see also Bett et al. 2007; Sharma & Steinmetz 2005). A spin parameter of $\lambda \simeq 0.05$ is characteristic of objects having negligible rotational support, and little systematic rotation (e.g., large elliptical galaxies and clusters of galaxies). Spiral and LSB galaxies are rotationally supported and in the case of LSBs $0.06 < \lambda < 0.21$ are LSBs (Jimenez et al. 1998; Boissier et al. 2003).

Apart from this source of angular momentum, originated by bulk motions and tidal fields, a random angular momentum, j , is generated by random velocities (see Ryden & Gunn 1987). In several of the papers which took account of angular momentum in SIM (e.g., Nusser 2001, Hiotelis 2002; Williams et al. 2004) only random angular momentum was taken into consideration. The approach usually followed was that of assigning a specific angular momentum at turn

around (e.g., Nusser 2001; Hiotelis 2002; Ascasibar, Yepes & Götteleber 2004), having typical value:

$$j = j_* \propto \sqrt{GM r_m} \quad (5)$$

The specific angular momentum, j , may be also expressed through the ratio $e_0 = \left(\frac{r_{min}}{r_{max}}\right)_0$, where r_{min} and r_{max} , are the pericentric and apocentric radii. Avila-Reese et al. (1998) used e_0 as a free parameter to take into consideration processes related to mergers and tidal forces that could produce tangential perturbations. In their paper, they showed that the detailed description of these processes is largely erased by the virialization process, remaining only through the value of e_0 , which they fixed to $e_0 = 0.3$. The value $e \simeq 0.2$ gives density profiles very close to the NFW profile (Avila-Reese et al. 1998, 1999). The previous procedure is based on results of N-body simulations of CDM halo collapse, giving constant $<\frac{r_{min}}{r_{max}}> \simeq 0.2$ ratios of dark matter particles in virialized haloes. An improvement to the previous model is due to Ascasibar, Yepes & Götteleber (2004), who found that particle orbits are slightly more radial as we move out to the current turn around radius, r_{ta} , and that there is a dependence on the dynamical state: major mergers are well described by constant eccentricity up to the virial radius, relaxed systems are more consistent with a power-law profile, while minor mergers are in the middle. A least-square fit to the relaxed population yields:

$$e(r_{max}) \simeq 0.8(r_{max}/r_{ta})^{0.1} \quad (6)$$

for $r_{max} < 0.1r_{ta}$.

In the present paper, random angular momentum is taken into account through Avila-Reese et al. (1998) method with the correction of Ascasibar, Yepes & Götteleber (2004).

Dynamical friction was taken into account as described in Antonuccio-Delogu & Colafrancesco (1994) (see also Appendix D of DP09). Its effects on structure formation were obtained by introducing the dynamical friction force in the equation of motion (Eq. A14 in DP09). We also took into account adiabatic contraction (AC) of dark matter halos in response to the condensation of baryons in their centers, and leading to a steepening of the dark matter density slope.

We summarize in the following the AC model taking also account of angular momentum exchange.

The present standard form of the AC model was introduced and tested numerically by Blumenthal et al. (1986) (see also Ryden & Gunn 1987; Barnes 1987; Oh 1990). Let's consider a spherically symmetric protostructure that consists of a fraction of baryons, $F_b = M_b/M_{500} \ll 1$, and a fraction $1 - F_b$ of dark matter particles constituting the halo. Here, M_{500} is the mass contained within a radius where the enclosed density is 500 times the critical density of the Universe, and $M_b = M_* + M_{gas}$, where M_* is the stellar mass and M_{gas} is that of gas. Baryons and halo particles are assumed to be well mixed initially (i.e., the ratio of their densities is F_b through the protostructure). As the baryons dissipatively cool and fall into a final mass distribution $M_b(r)$, a dark matter particle initially at radius r_i will move in to radius $r < r_i$, characterized by

$$r[M_b(r) + M_{dm}(r)] = r_i M_i(r_i) \quad (7)$$

where $M_i(r_i)$ is the initial total mass distribution, $M_b(r)$ is the final mass distribution of dissipational baryons and

M_{dm} is the final distribution of dissipationless halo particles. Assuming that the orbits of the halo particles do not cross, one obtains

$$M_{dm}(r) = (1 - F_b)M_i(r_i) \quad (8)$$

Eqs. (7), (8) can be iteratively solved to calculate the final radial distribution of the halo particles once $M_i(r_i)$ and $M_b(r)$ are given. A usual assumption is that initially baryons had the same density profile as the dark matter (Mo et al. 1998; Cardone & Sereno 2005; Treu & Koopmans 2002; Keeton 2001), and the final baryons distribution is assumed to be a Hernquist configuration (Rix et al. 1997; Keeton 2001; Treu & Koopmans 2002). In the present paper, the Blumenthal's model was improved following Gnedin et al. (2004) who proposed a simple modification which describes numerical results more accurately. They proposed a modified adiabatic contraction model based on conservation of the product of the current radius and the mass enclosed within the orbit-averaged radius:

$$M(\bar{r})r = \text{const.} \quad (9)$$

where the orbit-averaged radius is

$$\bar{r} = \frac{2}{T_r} \int_{r_{min}}^{r_{max}} r \frac{dr}{v_r}, \quad (10)$$

where T_r is the radial period.

The previous, AC model, assumes no angular momentum exchange between different components (e.g., baryons and DM). In the early phase of collapse, the baryons density is an order of magnitude smaller than that of DM, and the exchange of angular momentum has little impact on the dark matter. During the collapse baryons infall into the center of the proto-structure deepening the gravitational potential well. In the late stage of collapse the baryon density becomes large, non-axisymmetric component may develop due to the excitation of spiral waves and/or bar-like modes. The resulting increase of DM density acts as a sort of coupling process of the baryons and the DM (Klypin et al. 2001; Klypin, Zhao, and Somerville 2002). At later stages of collapse, when baryon density increases, the effect is potentially quite large resulting in a decrease of the dark matter density by a factor of ten (Klypin, Zhao, & Somerville 2002).

In order to describe quantitatively the quoted process, let's consider a spherical shell of dark matter with density ρ_{dm} , radius r , thickness dr , and specific angular momentum

$$j = rV_c = \sqrt{G[M_b(r) + M_{dm}(r)]r}. \quad (11)$$

one can get an implicit equation for the final radius r_f :

$$j_f = j \left[1 + \frac{A\Delta M}{4\pi\rho_{dm}r^3} \right], \quad (12)$$

$$A = 1 + \frac{r}{V_c} \frac{dV_c}{dr}, \quad (13)$$

$$\Delta M = M_{b,f} - M_b. \quad (14)$$

Klypin, Zhao, and Somerville (2002), where $M_{b,f}$ is the final baryons mass and $M = M_{dm} + M_b$ is the total mass inside a radius r . Eq. (12) is solved numerically. The solution also gives the mass inside a final radius r_f . Eq. (12) has the same structure as Eq. (7), the only difference is the term on the right-hand-side, which is the correction due to angular momentum deposition.

For what concerns baryons, we discussed how they were introduced in appendix E of DP09, and how their initial mass distribution and the final distribution were fixed. The quantity of baryons used in the calculation of Sect. 3.1, was fixed using Giodini et al. (2009) results. As shown from McGaugh et al. (2010) (see their Fig. 2), the fraction of baryons detected in all forms deviates monotonically from the cosmic baryon fraction as a function of mass. On the largest scales of clusters, most of the expected baryons are detected, while in the smallest dwarf galaxies, fewer than 1% are detected. The detected baryon fraction, f_d , is the ratio of the baryon fraction, $F_b = M_b/M_{500}$, and the universal baryon fraction, f_b , is

$$f_d = (M_b/M_{500})/f_b = F_b/f_b \quad (15)$$

where $f_b = 0.17 \pm 0.01$ (Komatsu et al. 2009). Note that in this paper the masses, M_{200} , and M_{vir} , are converted to M_{500} using the method used in White (2001), Hu & Kravtsov (2003), and Lukic et al. (2009).

In the four clusters studied in Sect. 3.2, we calculated the baryon fraction using Schmidt & Allen (2007) and checked that the result was in agreement with Giodini et al. (2009) results. More in detail, in this last case, we calculated the baryon content subtracting the total mass of clusters, obtained from the data in table 3 of Schmidt & Allen (2007), from the DM mass obtained from the data in their table 4, namely

$$M_b = M_{DM+b} - M_{DM} = \frac{800\pi}{3} \rho_c (r_{vir,DM+b}^3 - r_{DM}^3) \quad (16)$$

where ρ_c is the mean background (critical) density, and $r_{vir} = cr_s$, where the concentration parameter c , and the scale factor r_s are given in Schmidt & Allen (2007) for 34 massive, dynamically relaxed clusters of galaxies. Note, that Eq. (16) comes from the fact that for a NFW profile $M(r = r_{vir}) = \frac{800\pi}{3} \rho_c r_{vir}^3$.

In order to have a more clear view of how the previous quoted processes works to build up the cluster, we summarize the structure formation starting from high redshifts. Initially the proto-structure is in the linear phase, it expands, reaches a maximum of expansion and then collapses. Baryons trapped inside the potential wells of DM halos are subject to radiative dissipation processes which give rise to clumps and self-gravitating clouds before it collapses to the halo center and condenses into stars and galaxies. The stage of baryons cooling and stars formation happens as described in Ryden (1988) (Sect. 4: "baryonic dissipation"). In the infall, the baryons compress the DM halos (AC), producing a steepening of the DM density profile. When clumps reaches the central high density regions they experience a dynamical friction force from the less massive DM particles as they move through the halo. Dynamical friction acts as an angular momentum engine (Tonini, Lapi & Salucci 2006), and energy and angular momentum are transferred to DM (El-Zant et al. 2001, 2004), increasing its random motion, and giving rise to a motion of DM particles outwards⁴. More-

⁴ Another model of baryon-DM interaction, and exchange of angular momentum between the baryons and DM was previously discussed in this section (Klypin et al. 2001; Klypin, Zhao, & Somerville 2002).

over, ordered angular momentum mainly acquired in the expansion phase, through tidal torques, gives rise to nonradial motions in the collapse phase that amplifies the effects of the previous mechanism. Then the joint effect of angular momenta (ordered and random) and dynamical friction, transporting it from baryons to DM, overcomes that of the AC and the profile starts to flatten.

As previously described, in order to follow the structure formation, the protostructure is divided into mass shells, containing DM and baryons, which after radiative dissipation forms clumps, stars, and galaxies. In order to form the structure the evolution in various phases is followed by means of the SIM. After turn-around shells move inward, baryons (namely, baryonic clumps) exchange angular momentum with DM and accretes to the center, forming the central galaxy (BGC) (see also Lackner & Ostriker 2010).

As already shown in DP09, and DP12, the density profiles, obtained with the model summarized in this section, and fully described in DP09, DP12, produces profiles in agreement with other studies (e.g., El-Zant et al. 2001, 2004; Mashchenko et al. 2005, 2006, 2007; Romano-Diaz et al. 2008, and the more recent paper of Governato et al. 2010).

3 RESULTS AND DISCUSSION

3.1 Changes of density profiles with baryons fraction and angular momentum

As discussed in the introduction, dwarf galaxies and LSBs have rotation curves incompatible with the haloes that Λ CDM model predicts. This problem, known as Cusp-Core problem, pointed out by Flores & Primack (1994), and Moore (1994) has not seen till now a clear-cut solution.

Inner density profiles in clusters of galaxies have also been at the center of a similar debate to that of dwarfs, with claims of value of α going from $\alpha = 0.35$ (S02) to $\simeq 1.9$ (Arabadjis, Bautz & Garmire 2002).

To this aim, in the following of the paper, we use DP09 to generate density profiles in the range $10^{14} - 10^{15} M_{\odot}$, then focalizing our attention on changes of inner density profiles produced by different values of baryon fraction and random angular momentum.

In Sect. 3.1, and 3.2 the baryon fraction was obtained as described in the final part of Sect. 2. Ordered angular momentum is fixed to typical values obtained by Gottlöber & Yepes (2007), and random angular momentum is used as a parameter.

The results of our calculation are plotted in Fig. 1a-c. The ordered angular momentum used to obtain the solid line in Fig. 1a-1c (obtained by the tidal torque theory as in DP09) is characterized by $\lambda = 0.03^5$. The baryonic fraction is $F_{B_*} = M_b/M_{500} = 0.15$, or $f_d = F_b/f_b \simeq 0.88$ (see McGaugh et al. 2010), and the typical random angular momentum is j_* . The solid line in Fig. 1a-c is obtained using these typical values. The solid line, obtained as described is chosen as the reference halo.

Differently from DP12, in the present paper, we will

study the change of the inner density profile slope just when the random angular momentum changes, since differently from dwarf and spiral galaxies, clusters of galaxies are nonrotationally supported (the mean rotational velocity, and ordered angular momentum of most luminous clusters are much less than their velocity dispersions).

In fig. 1a, we fix the value of f_d to the value previously discussed, and vary the amplitude of the random angular momentum, j . The short-dashed (dotted) line in Fig. 1a, represents the case $j = j_*/1.5$ ($j = j_*/2$), where j_* is the value of j for the reference case (solid line). As expected, the density profile steepens when j decreases ($\alpha \simeq 0.6$ (solid line), 0.75 (short-dashed line), 0.95 (dotted line)). This steepening of the profile with j agrees with several previous results (Sikivie et al. 1997; Avila-Reese et al. 1998; Nusser 2001; Hiotelis 2002; Le Delliou & Henriksen 2003; Ascasi-bar, Yepes & Göttleber 2004; Williams et al. 2004). The long-dashed (dot-dashed) line in Fig. 1a, represents the case $j = j_* \times 1.5$ ($j = j_* \times 2$). As expected, larger values of j produce flatter profiles ($\alpha \simeq 0.4, 0.2$, for the long-dashed, and dot-dashed line, respectively).

Fig. 1b, is the same as Fig. 1a, but the halo mass is in this case $10^{15} M_{\odot}$. Short-dashed (dotted) line is characterized by $\alpha \simeq 0.93$ (1.05), while long-dashed (dot-dashed) line is characterized by $\alpha \simeq 0.52$ (0.32).

A comparison of Fig. 1a and Fig. 1b, shows that the $10^{14} M_{\odot}$ halo is less steep than the $10^{15} M_{\odot}$ one. The steepening of the cusp with mass is in agreement with previous studies (Cen & Ostriker 2000; Ricotti 2003). Both Fig. 1a and Fig. 1b, show that haloes with higher angular momentum have smaller inner slopes. The steepening of the profile with mass is due to the fact that higher density peaks (larger ν^6) are usually progenitors of more massive haloes⁷ which are characterized by a larger central density contrast. As a consequence, a generic shell inside this peak will fill more strongly the central potential and will expand less than if it was located in a smaller density peak. The angular momentum acquired during expansion will be reduced and haloes will be more concentrated. It is important to notice that the quoted trend of increased central concentration as a function of mass applies only to haloes that started out as peaks in the density field smoothed with a fixed R_f scale (see Appendix B of DP09). Our conclusions do not mean that, for example, clusters of galaxies will be more centrally concentrated than galaxies, since different smoothing scales would apply in the two cases. The angular momentum dependence of the slope arises from the fact that less massive objects are originated from peaks having a smaller height. They

⁶ $\nu = \delta(0)/\sigma$, where δ is the mean fractional density excess inside a shell, and σ is the mass variance filtered on a scale R_f (see Appendix B of DP09).

⁷ As discussed by Peacock & Heavens 1990; Del Popolo & Gambera 1996 or Gao & White (2007) (Fig.1), modelling the peaks as triaxial spheroids one obtains a peak mass $M = \frac{2^{3/2}(4\pi/3)\rho_b R_*^3}{\gamma^3 + (0.9/\nu)^{3/2}}$ for $0.5 \leq \gamma \leq 0.8$ (where γ and R_* are spectral parameters given by Eq. (B6 and B7) in DP09). The peak mass is an increasing function of ν . It is reasonable that lower ν peaks should have lower mass; peaks with $\nu \simeq 0$ will tend to sit in regions of larger scale underdensity (cancelling the small-scale overdensity), and hence the $\sim \rho_c R_*^3$ of material, which initially surrounds the peak, may not be accreted following central collapse.

⁵ Note that even if we studies haloes of mass in the range $10^{14} - 10^{15} M_{\odot}$, and this imply differences in ordered angular momentum, the spin parameter, λ has small differences.

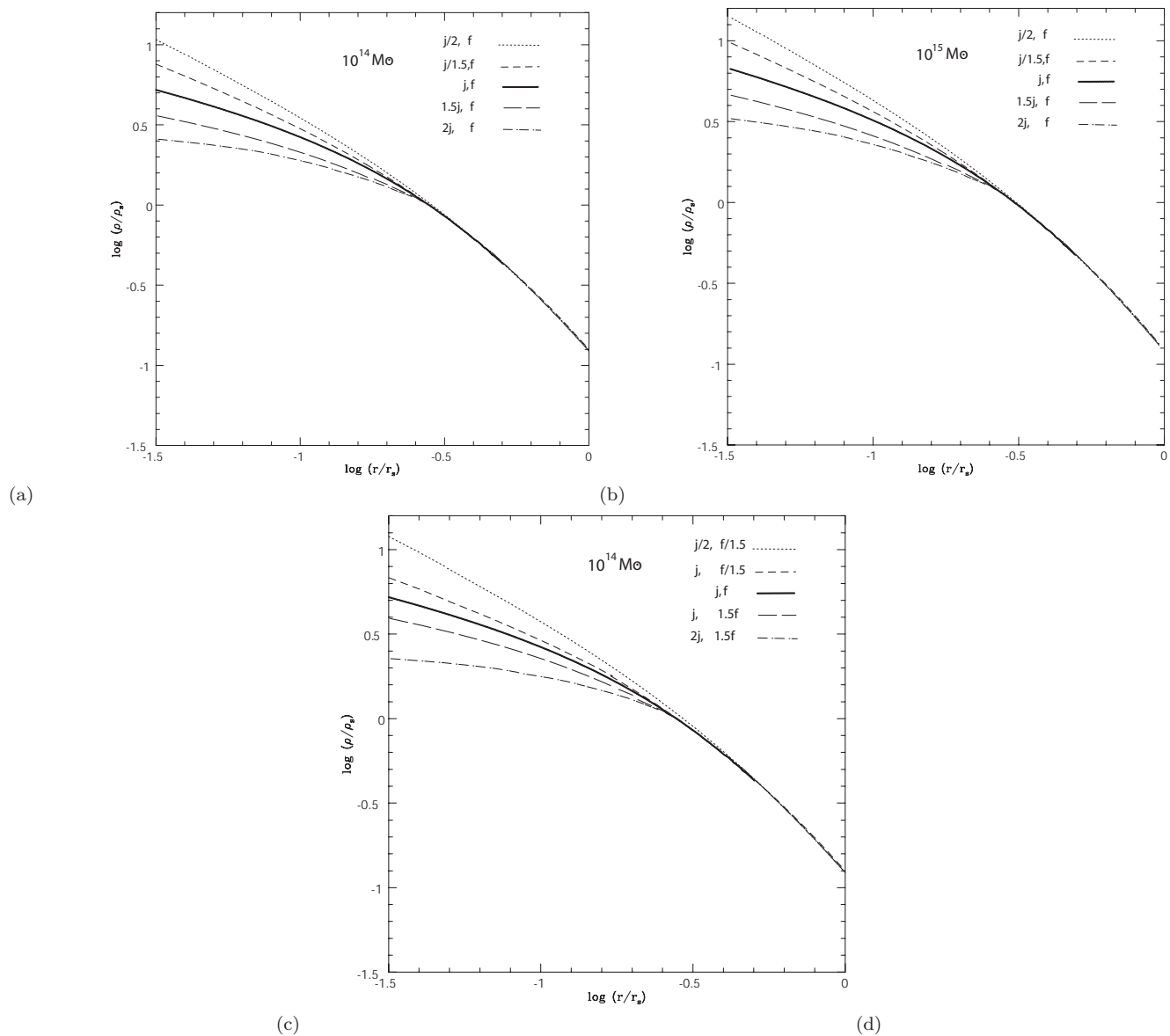


Figure 1. Changes of the density profile with baryonic fraction and random angular momentum j . Panel (a) refers to density profiles with mass $10^{14} M_\odot$ varying only j . The solid line is characterized by $F_{B_*} = M_b/M_{500} = 0.15$ ($f_{d_*} = 0.88$), and $j = j_*$. The upper short-dashed line, and the dotted line are characterized by $f_d = f_{d_*}$, and $j = j_*/1.5$, and $f_d = f_{d_*}$, $j = j_*/2$, respectively. The long dashed line, and dot-dashed line, are characterized by $f_d = f_{d_*}$, and $j = j_* \times 1.5$, and $f_d = f_{d_*}$, $j = j_* \times 2$, respectively. Panel (b), represents the density profile for haloes of mass $10^{15} M_\odot$. Panel (c) plots density profiles for haloes of mass $10^{14} M_\odot$ varying both j and baryonic fraction. The solid line, short-dashed line, dotted line, are characterized by $f_d = f_{d_*}$, $j = j_*$; $f_d = f_{d_*}/1.5$, $j = j_*$; $f_d = f_{d_*}/1.5$, $j = j_*/2$, respectively. The long-dashed line, dot-dashed line, are characterized by $f_d = 1.5 \times f_{d_*}$, $j = j_*$; $f_d = 1.5 \times f_{d_*}$, $j = j_* \times 2$, respectively.

acquire less ordered, h , and random, j , angular momenta (Ryden & Gunn 1987). The larger is the angular momentum, the more particles constituting the shell will remain closer to the maximum radius, producing a flatter density profile. Summarizing, particles having larger h and j tend to live far from the center, so not contributing to the central density. At the same time, a larger value of mass produces an increase of the central density contrast, and a steeper profile.

The baryon content of the halo is another parameter playing a key role in shaping density profiles. In Fig. 1c, we studied how changes in the baryonic fraction change the

profile of a $10^{14} M_\odot$ halo. Similar results, not plotted, are valid for $10^{15} M_\odot$ haloes.

In Fig. 1c, the solid line is the same as Fig. 1a, while the short-dashed (dotted) line represents the case $f_d = f_{d_*}/1.5$ and $j = j_*$ ($f_d = f_{d_*}/1.5$ and $j = j_*/2$), where $f_{d_*} = F_{B_*}/f_b = 0.15/0.17 = 0.88$. The long-dashed (dot-dashed) line represents the case $f_d = f_{d_*} \times 1.5$ and $j = j_*$ ($f_d = f_{d_*} \times 1.5$ and $j = j_* \times 2$).

The short-dashed line shows that a decrease of the baryonic fraction, from f_{d_*} to $f_{d_*}/1.5$ produces a steepening of the density profile, to $\alpha \simeq 0.7$. If also j is decreased, to $j_*/2$, a further steepening of the profile is produced ($\alpha \simeq 1.1$). In

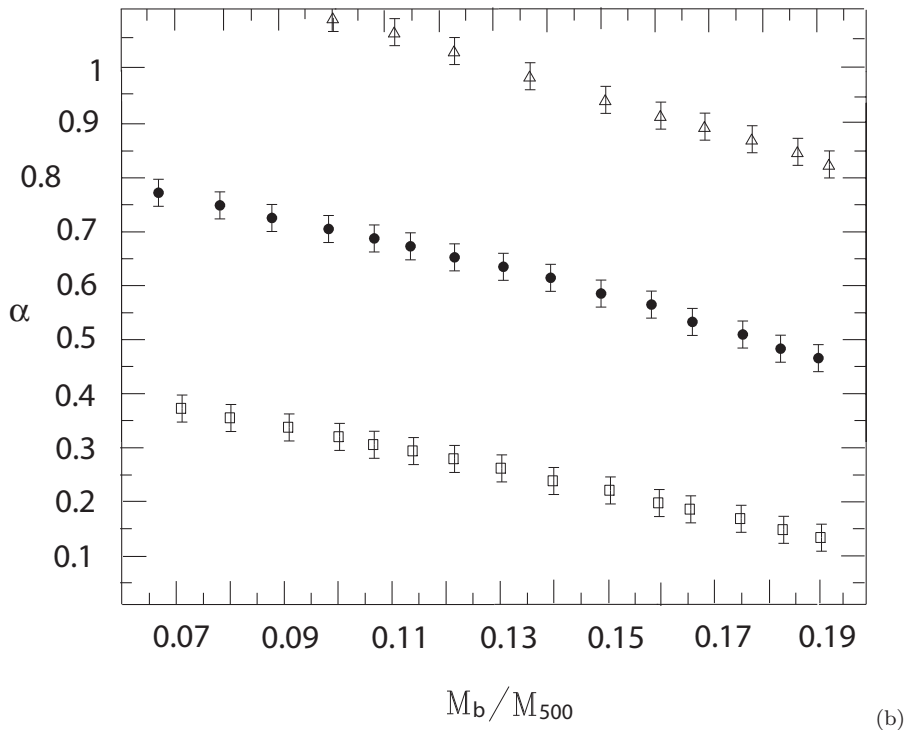


Figure 2. Changes of the inner slope α in terms of the ratio of baryonic to total mass, M_b/M_{500} . Dots with error-bars refer to the case $f_d = f_{d*}$, $j = j_*$. The triangles with 1σ error-bars refers to the case $f_d = f_{d*}$, $j = j_*/2$, and the squares with error-bars to the case $f_d = f_{d*}$, $j = j_* \times 2$.

the reverse case, the long-dashed line, representing the case $f_d = f_{d*} \times 1.5$ and $j = j_*$, the profile flattens ($\alpha \simeq 0.35$), and a further flattening of the profile is produced ($\alpha \simeq 0.1$ if also, j is increased to $j = j_* \times 2$). The clear tendency to have flatter inner profiles for larger baryon content is connected to the fact that the presence of a larger quantity of baryons guarantees a larger transfer of energy and angular momentum from baryons to DM with the results that DM moves to larger orbits reducing the inner density. It is important to notice, that an increase in angular momentum has a more important effect on the inner density profile slope than an increase in the baryon fraction (an increase of a factor of 2 in random angular momentum has a larger effect than an a similar increase in the baryon fraction).

In the case that the system does not contain baryons, like dissipationless N-body simulations, the density profile converge to the Einasto profile (as shown in Fig. 1d of DP09), characterized by a logarithmic slope that varies continuously with radius (Navarro et al. 2004, 2010).

In Fig. 2, we plot how the negative logarithmic slope of the DM density at small radii ($10^{-2}r_{vir}$), $\alpha = \frac{d \log \rho}{d \log r}$, varies with the baryonic content in haloes, M_b/M_{500} . The dots with 1σ error-bars represent the relation α - M_b/M_{500} in the case $f_d = f_{d*}$ and $j = j_*$. The plot shows a decrease of α with increasing value of the baryonic fraction, f_d , as already noticed in Fig. 1: the final density profiles are shallower when F_b (or similarly f_d) is higher. The triangles (squares) with 1σ error-bars, represent the same relation in the case $f_d = f_{d*}$ and $j = j_*/2$ ($f_d = f_{d*}$ and $j = j_* \times 2$). The plot shows that for a given f_d one can obtain different slopes according to the value of random angular momentum of the system, and this suggests that the cluster mass and

baryonic fraction are not the only fundamental parameters in shaping the density profile. A fundamental role is played by the orbital properties of the objects constituting the cluster. Galaxies moving on different orbits heat the DM at different rates. Galaxies having larger kinetic energy transfer, through dynamical friction, a larger amount of energy to DM. So, if baryon content has a certain importance in determining the final DM distribution, the orbital parameters of galaxies and their dynamics has a similar or even a larger importance. In a recent paper, Laporte et al. (2012) studied how the evolution of galaxies influence clusters of galaxies formation. They followed galaxies evolution through collisionless mergers and found that cusps with $0.8 < \alpha < 1.3$ can be flattened to $0.3 < \alpha < 0.9$ at the innermost resolved radii. This result is in qualitative agreement with the results of our paper. However, in their study, the density profiles depend not only on the orbital properties of galaxies, as in the present study, but also on the internal structure of galaxies. Less tightly bound galaxies (i.e., less compact) are more easily stripped with respect to more tightly bound ones, and as a result the more is the quantity of less compact galaxies in the cluster the more quantity of stellar mass is stripped and deposited on the BCG. The effect on the slope of the DM profiles is that clusters containing more compact galaxies have shallower inner profiles and vice versa. Even if the model is an improvement on that of El-Zant et al. (2004), it has several limitations as recognized by the authors, and certain aspects of matter distribution in their simulations are unrealistic. This is one of the reasons they did not even attempt to reproduce observations of clusters. Moreover, the flattening of the inner slope of the density profile of clusters is not only due to the effect of galaxy evolution. Dissipa-

tional processes have an important role in shaping galaxies at early times. Baryons are more important than DM in the inner parts of galaxy clusters and alter the DM profile in many ways, as described in the previous part of the present paper.

In Fig. 1, and Fig. 2, we discussed how angular momentum shapes the density profiles, and that haloes characterized by a larger angular momentum have flatter density profiles. This result could erroneously lead us to think that angular momentum is the primary effect driving the shaping of the density profiles, and the principal reason giving rise to the difference between density profiles found in simulations and those found in the present paper. This is not the case. We have to recall that even if we are studying the effect of angular momentum change on the inner density slope, our system is composed of baryons and DM, and as a consequence our results are different from dissipationless N-body simulations. In our model, angular momentum is not working alone in shaping the density profiles, dynamical friction transfer angular momentum from baryons to DM. The larger is the angular momentum in the system, the larger is the quantity that can be transferred to DM with a consequent larger flattening of the density profile. I want also to add that the flattening of density profiles with increasing magnitude of angular momentum was also obtained in several studies even of systems not containing baryons (Avila-Reese et al. 1998, 2001; Subramanian et al. 2000; Nusser 2001; Hioteles 2002; Le Delliou & Henriksen 2003; Ascasibar, Yepes & Göttleber 2004; Williams et al. 2004; Ascasibar, Hoffman & Gottlober 2007). In peculiar, Ascasibar, Yepes & Göttleber (2004), compared the analytical profiles of SIM which included non-radial motions with a set of high-resolution N-body simulations, showing that angular momentum is responsible for the shape of the density profile near the centre. Ascasibar, Hoffman & Gottlober (2007) used N-body simulations to show that SIM gives density profile in good agreement with N-body simulations and that larger values of angular momentum produce a flattening of the profile.

Angular momentum acts also on galaxies, and if it was the only effect taken into account in our model, it would delay their collapse, keeping them away from the center. In reality galaxies, as baryons, are also subject to dynamical friction which makes them lose their energy and sink to the center (Kashlinsky 1987).

The reason why our model gives different results from dissipationless N-body simulations was already discussed in DP09, and it is not connected to the way our model takes account of angular momentum. The issue is not if our model takes into account angular momentum more reliably than N-body simulations, but the difference among the system described in our model and that of dissipationless simulations. In DP09 (beginning of page 2101), we described the two-fold effect of baryons presence, namely the steepening of the density profile due to AC and the flattening of the inner density profile due to the transfer of angular momentum from the baryons to the DM. In collisionless N-body simulations, in which baryons are not present, this complicated interplay between different effects is not taken into account. Only recent SPH simulations (Romano-Diaz et al. 2008; Governato et al. 2010) took account of the baryonic component, finding the quoted cusp erasing.

Finally, we recall that a check of the model against the Governato et al. (2010) SPH N-body simulations, has been performed in DP12 (Fig. 3).

3.2 Comparison with observed clusters of galaxies

At this point, we compare the results of our model with density and mass profiles of observed clusters, ranging from a flat inner profile, namely that of A611, to intermediate ones, namely A383, to steep profiles, namely MACSJ1423.8+2404 and RXJ1347.5-1145.

A611, A383, and RX J1133 are three of the clusters studied in a series of papers of Sand (S02, S04, and S08) and Newman (N09, N011). The quoted papers, followed a proposal of Miralda-Escude (1995), evidencing that if for a cluster we can add to the information on tangential and radial arc the information concerning the potential of the central galaxy (BCG), stronger constraints on the inner profiles of DM and luminous components can be obtained. S02 studied MS 2137-23, while S04 six clusters (MS2137-23, A383, A963, RX J1133, MACS 1206, and A1201), and S08 improved the results concerning MS2137-23 and A383. N11 improved the constraints previously obtained in S08 concerning A383, and N09 studied A611.

3.2.1 A611

A611 has been studied in several papers (OWLS team; Bonamente et al. 2004; Schmidt & Allen 2007; Hurley-Walker et al. 2011 (AMI consortium)). N09, combined weak lensing from multicolor *Subaru* imaging, strong lensing (*Hubble Space Telescope*), and stellar velocity dispersion measures (Keck Telescope), sampling the dark matter profile from $\simeq 3$ kpc to 3.25 Mpc. In order to accurately compare observational data and N-body simulations, one needs a) to separate DM from baryons, which, nevertheless they are a small part of the total mass of clusters, are usually dominating in the inner kpc scale; b) to probe mass on all scales. To this aim it is necessary to consider a wide dynamic range in radius. Concerning the mass distribution in the range 150 kpc- 3.25 Mpc, N09 found values of $r_s = 320_{-110}^{+240}$ kpc, and $c = 5.1_{-1.6}^{+1.7}$ (in agreement with Schmidt & Allen 2007). The distribution of the stellar mass of BCG, measured through strong lensing and stellar velocity dispersions, is well fitted by a $R^{1/4}$ law in the 3-20 inner kpc. The BCG is characterized by $L_B = (5.6 \pm 0.8) \times 10^{11} M_\odot$, and $M_{*,BCG}/L_B = 2.7_{-0.8}^{+0.7}$ (N09). Combining weak lensing, strong lensing, and stellar kinematics data, then they concluded that $\alpha < 0.3$, (< 0.56 , < 0.65) at 68%, (95%, 99%) CL. Schmidt & Allen (2007) found a value of the slope $\alpha = 0.64^{+0.94}$. An important result obtained by N09 is that using a subset of their data coming from just one technique (e.g., weak lensing, or strong lensing), the data are well fitted by a NFW model, but NFW model is unable to fit all data simultaneously. This imply the need to use several combined techniques and large radial scales. We compared the result of our model to N09 DM density profile in Fig. 3a. The cluster mass is estimated as $M_{vir} = 6.18_{-1.81}^{+3.82} \times 10^{14} h^{-1} M_\odot$ (Schmidt & Allen 2007), $M_{200} = 5.6_{-2.7}^{+4.7} \times 10^{14} h^{-1} M_\odot$ (Romano et al. 2010). We recall, that, as previously reported, all masses in the paper were converted to M_{500} . In order to

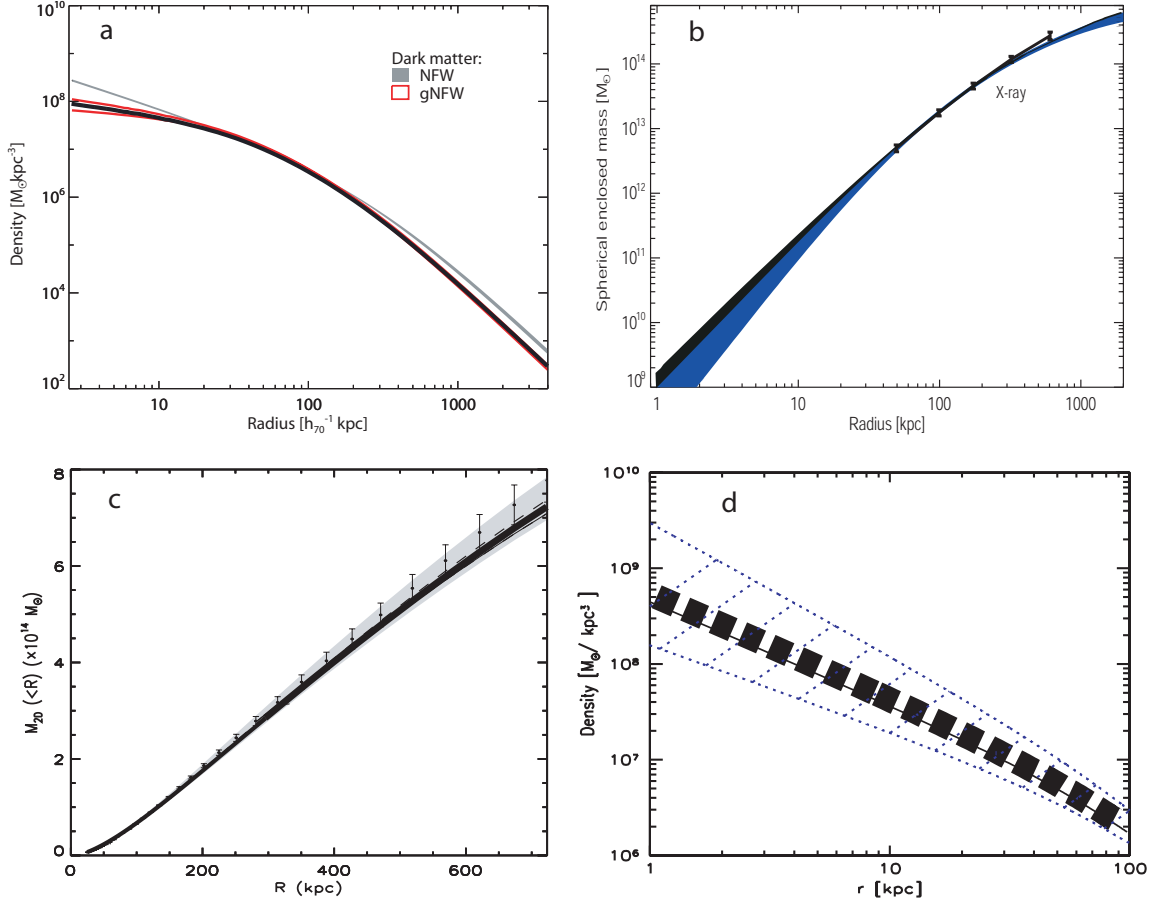


Figure 3. Fig. 3a plots the density profile of A611. The grey solid line is the NFW profile, the red lines bracket the 68% confidence region of the density profile obtained by N09, while the black band is the result of our model. Fig. 3b represents the mass profile of A383. The blue band is the observational result of N11, while the black band the mass distribution obtained with our model. Fig. 3c represents the mass profile of MACS J1423. The azure band with errorbars is the observational result of Morandi, Pedersen & Limousin (2010), while the black band is the result obtained with our model. Fig. 3d represents the density profile of RX J1133. The solid curve and the shaded region are the S04 observational result. The black dashed band is the result of our model. The confidence regions in Fig. 3a-c are 1σ while those in Fig. 3d are 2σ .

determine the DM density profile, we used our model. The baryonic fraction obtained as described in the final part of Sect. 2, gives a value of $M_b/M_{500} \simeq 0.15$ ($f_d \simeq 0.88$). The value of the baryonic fraction is larger with respect to that of RX J1133, and MACS J1423 (as we shall see in the following), and this is one reason why one should expect a flatter inner profile with respect to the two quoted clusters, well fitted by a NFW model. In Fig. 3a, the grey line is the NFW fit, the red lines bracket the 68% confidence region of the density profile obtained by N09, while the black band is the result of our model (68% CL). Looking at Fig. 1b, for a cluster having a mass $\simeq 10^{15} M_\odot$ and $f_d = f_{d*}$, and $j = j_*$, the inner slope is of the order of 0.7. Taking account the fact that A611 has a mass smaller than $10^{15} M_\odot$, one would obtain a value of $\alpha \simeq 0.65$. In order to obtain the good fit plotted in Fig. 3a, we had to increase the magnitude of j to $2 \times j_*$. As shown in Fig. 1, and also in Williams et al. (2004) (Fig. 6), increasing the value of j produces a flattening of the profile.

3.2.2 A383

A383, is one of the most X-ray luminous clusters in the redshift slice $0.17 < z < 0.26$, at $z = 0.189$. It is characterized by numerous strong lensing features and a dominant central galaxy. An analysis of the mass distribution in the core, built up through a lens model of the cluster, was carried out by Smith et al. (2001, 2005). The inner density profile, was evaluated by them to be $\alpha = 1.3 \pm 0.04$. The cluster was one of the quoted six clusters studied in S04, combining results from stellar velocity dispersion data, and lensing. The cluster has both a radial and tangential arc. The dispersion velocity profile, and the density profile are plotted in Figs. 7, 8 of S04. The inner DM slope obtained by S04 was $\alpha = 0.38^{+0.06}_{-0.05}$ ($^{+0.12}_{-0.12}$) (68% (95%) CL). The results of S04, and consequently the constraints on A383 inner slope, were criticized by Meneghetti et al. (2007)⁸, on the base

⁸ Notice that Meneghetti uses triaxial clusters similar to those obtained in simulations, while those in S04 are more spherical.

that S04 used axially symmetric models in order to obtain a description of the six clusters mass model, while a pseudo-elliptical lens model (including ellipticity in the lensing potential) gives rise to steeper density profiles. The previous criticisms were tackled in S08, in the case of A383, finding again a flat inner DM slope ($\alpha = 0.45_{-0.25}^{+0.2}$).

A further improvement to the model was presented in N11, in which the authors, used the same technique used in N09. They also combined X-ray and lensing constraints, in order to measure the DM elongation along the line of sight. In this way, it was further possible to tackle an important systematic uncertainty in the mass profile determination (see Morandi et al. 2010). As a result, they further improved the S08 constraints, who has not taken into account triaxiality. They obtained a value of $\alpha < 0.70$ (68% confidence), $\alpha < 1$ (95% confidence), and a best fit (inferred from weak, strong lensing, kinematics, and X-ray data) of $\alpha = 0.59_{-0.35}^{+0.30}$.⁹ In order to compare the mass profile obtained by N11, with our model, we need mass and baryonic content of the cluster. Zitrin et al. (2011) and Schmidt et al. (2007) found values of $M_{vir} = 6.26_{-0.25}^{+0.26} \times 10^{14} h^{-1} M_{\odot}$, and $M_{vir} = 6.87_{-1.85}^{+1.89} \times 10^{14} h^{-1} M_{\odot}$, respectively. The mass of the BCG, within $\simeq 19$ kpc, is $1.14 \pm 0.03 \times 10^{12} M_{\odot}$ (Zitrin et al. 2011) in agreement with N11. The baryonic fraction was obtained as for A611. The value of M_b/M_{500} is $\simeq 0.15$ ($f_d \simeq 0.88$). In Fig. 3b, we compare the mass distribution obtained with our model (black band), with that of N11 (blue band). The good fit to the mass distribution of A383 is obtained with the typical value j_* of random angular momentum. This shows that even if A383 has a mass and baryonic fraction close to that of A611, the smaller value of j give rise to the steeper profile observed ($\alpha \simeq 0.6$).

3.2.3 MACSJ1423.8+2404

The cluster of galaxies MACS J1423.8+2404 (in the following referred as MACS J1423), is a triaxial¹⁰ massive ($M = 4.52_{-0.64}^{+0.79} \times 10^{14} M_{\odot}$, Schmidt & Allen 2007) strong cooling core source¹¹ (Morandi et. al. 2007b) at $z = 0.539$. It is very relaxed (Kartaltepe 2008) with very low central temperature (~ 2 keV). Morandi, Pedersen & Limousin (2010) performed a joint analysis (X-ray, strong, and weak lensing) to determine DM density profile and ICM parameters. The BCG mass is $5 \times 10^{11} M_{\odot}$. The three-dimensional analysis of the cluster, lead (Morandi, Pedersen & Limousin 2010) to measure an inner slope $\alpha = 0.94 \pm 0.09$ smaller than the two-dimensional spherical modeling, giving a value of $\alpha = 1.24 \pm 0.07$. Similarly to the previous clusters, we used our model to determine the mass profile of the cluster. The value of the baryonic fraction, inferred as in A383, and A611, gives $F_b \simeq 0.1$ ($f_d \simeq 0.59$), and the mass profile, plotted in Fig. 3d (black band), in good agreement with Morandi, Pedersen & Limousin (2010) (azure band with errorbars), was obtained assuming $j = j_*/1.5$. The effect of steepening of

⁹ The authors are also studying other nine clusters with the same level of precision.

¹⁰ DM halo axial ratios are 1.53 ± 0.15 , on the plane of the sky, and 1.44 ± 0.07 , along the line of sight (Morandi, Pedersen & Limousin 2010).

¹¹ i.e., the central cooling time is much smaller than the age of universe.

the profile with decreasing j was pointed out by Williams et al. (2004) (their Fig. 6). Reducing the angular momentum of dark matter particles, reduces random velocities which results in steeper central density slopes.

3.2.4 RX J1133

RX J1133 accurately studied in S04, is a cluster with total mass $\simeq 3.2 \times 10^{14} M_{\odot}$ (Cardone, Piedipalumbo, & Tortora 2005; Lackner & Ostriker 2010 (private communication)), and a BCG with mass $3 \times 10^{11} M_{\odot}$ (Lackner & Ostriker 2010 (private communication)). S04 identified a tangential and radial arc and measured the velocity dispersion profile of the BCG. S04 disentangled the DM and baryonic component, finding density profiles of DM, luminous matter, and total matter (see S04, Fig. 8). The inner slope of the DM profile was found consistent with that of a NFW profile ($\alpha = 0.99_{-0.14}^{+0.18}$). In Fig. 3d, we plot the DM density profile of RX J1133. Fig. 3d represents the density profile of RX J1133. The solid curve and the shaded region is the S04 observational result. The black dashed band is the result of our model, using the previously given mass for the cluster, and the baryonic fraction calculated as for the previous three clusters. The obtained value $F_b \simeq 0.1$ is smaller than that of A383 and A611, implying a steeper slope with respect to the two quoted clusters. The model of this paper gives a very good fit to the DM density profile of RX J1133, obtained by S04, if $j = j_*/2$. The reduction of random angular momentum is justified as in the case of MACS J1423. Finally, we notice how the result shows that a NFW model is also a good fit to RX J1133 density profile.

The confidence regions in Fig. 3a-c are 1σ while those in Fig. 3d are 2σ .

4 DISCUSSION

4.1 What are the origins of the differences?

From the results of the previous sections, we arrive to two important conclusions, that we will discuss: a) not all clusters density profiles are fitted by the NFW model. Some of them have flat inner density profiles (e.g., A611), some have intermediate slopes, between pseudo-isothermal profiles and NFW profiles, (e.g., A383), and others are well fitted by NFW profiles (e.g., RX J1133); b) the Λ CDM model is unable to describe the density profile of some clusters.¹²

In connection with the first conclusion, a connected question is the following: what is the cause of the differences of density profiles in clusters? In the study of the role of baryons and random angular momentum developed in Sect. 3.1, we saw that the causes that give rise to different slopes in clusters are three, namely the mass (clusters with larger mass have steeper profiles), the baryon content (clusters richer in baryons have flatter profiles), and random angular momentum, j (larger values of j implies flatter profiles). We also saw that random angular momentum have a stronger role than baryons in shaping density profiles. A383 and A611 have a similar mass ($M_{vir} \simeq 6 \times 10^{14} h^{-1} M_{\odot}$), and a similar baryonic fraction ($F_B \simeq 0.15$ ($f_d \simeq 0.88$)).

¹² Obviously issue a, and b are strictly connected.

RX J11333 and MACS J1423 have slightly smaller masses ($\simeq 3 - 4 \times 10^{14} h^{-1} M_{\odot}$), and smaller baryonic fraction ($F_B \simeq 0.1$ ($f_d \simeq 0.59$)). The difference in baryonic fraction is one of the cause of the steeper profile of RX J11333 and MACS J1423 with respect with the other two clusters, in agreement with observations. We should also not forget that, similarly to dwarf galaxies, in order two clusters have a similar density profile, it is not only important that the baryonic fraction is similar for the two objects, but the way baryons are distributed has also an important role.

In particular, the larger or smaller concentration of gas and stars in the central $\simeq 10$ kpc, in the BCG, is also important. As shown by Schmidt & Allen (2007) (Fig. 4), the inner slope of clusters of galaxies (MS 2137.3-2353, in particular) decreases with increasing values of the central mass. In the inner $\simeq 10$ kpc, A611 has a $M_{BCG}/M_{vir} \simeq 0.004$, using the data of N09, and of Schmidt & Allen (2007), concerning M_{BCG}/M_{vir} . A383 has $M_{BCG}/M_{vir} \simeq 0.002$ (within $\simeq 19$ kpc), using N11; Schmidt & Allen (2007), and Zitrin et al. (2011), data. RX J1133 has $M_{BCG}/M_{vir} \simeq 0.001$ (Cardone, Piedipalumbo, & Tortora 2005; Lackner & Ostriker 2010 (private communication)), and MACS J1423 has a similar value. The larger value of ratio of the inner stellar mass to total mass of A611 with respect to A383, and the larger ratio of A611, and A 383 with respect to RX J1133 also implies that the inner slope of A611 is flatter than that of A383, and flatter than those of MACS J1423, and RX J1133.

It is interesting to discuss more in detail the role of the total baryonic mass, M_b , and the central one. As shown in El-Zant et al. (2001, 2004), Romano-Diaz et al. 2008, DP09, Governato et al. (2010), baryons presence produces in general a flattening of the density profile. The baryon diffused component produces rounder halos and less triaxial halos than those seen in DM simulations (Gustafson et al. 2006; Debattista et al. 2008; Abadi et al. 2010), and this change of shape has also influence on dynamical mass estimate (N09). The final configuration of a cluster is fixed by the initial quantity of baryons present in the proto cluster and by collapse/formation process.

From this considerations, we should expect, in hierarchical formation models, that the final central baryonic content and the BCG mass is somehow correlated with baryonic and total cluster mass. This is in fact the case, as shown by Whiley et al. (2008), who using the models of de Lucia & Blaizot (2007), found that $M_{BCG} \propto M_{cl}^{0.4}$ or $M_{cl}^{0.5}$ depending on the feedback model used. Also a correlation between BCG luminosity and cluster X-ray luminosity was found by several authors (Schombert 1988; Edge 1991; Edge & Stewart 1991; Hudson & Ebeling 1997). Whiley et al. (2008) measured the quoted correlation as $M_{BCG} \propto M_{cl}^{0.12 \pm 0.03}$ for K band magnitudes inside a diameter of 37 kpc (radius of $13 h^{-1}$ kpc). Brough et al. (2008) found $L_{BCG} \propto M_{cl}^{0.11 \pm 0.10}$ at K band inside $12 h^{-1}$ kpc (several other results are given in Lin & Mohr 2004; Popesso et al. 2007; Yang et al. 2008; Haarsma et al. 2010).

In Fig. 4a, we calculated the baryonic mass in the inner 10 kpc and plotted it against the total mass. The dots with 1σ errorbars represent the quoted relation for $f_d = f_{d*}$ and $j = j_*$. The triangles with errorbars represent the quoted relation for $f_d = f_{d*}$ and $j = j_* \times 2$. The squares with

errorbars represent the quoted relation for $f_d = f_{d*}$ and $j = j_*/2$. The plot shows a similar correlation as that found in Whiley et al. (2008)

$$\frac{M_{b,in}}{10^{11} M_{\odot}} \simeq 1.3 \times 10^6 \left(\frac{M_{500}}{10^{14} M_{\odot}} \right)^{0.4} \quad (17)$$

Fig. 4b, plots the inner slope (defined as in Fig. 2) in terms of the ratio $M_{b,in}/M_{500}$. Dots with 1σ error-bars represent the quoted relation in the case $f_d = f_{d*}$ and $j = j_*$.

In Fig. 4b, it is also important to note that the fundamental parameter influencing the inner slope of the density profile is $M_{b,in}/M_{vir}$ and not just the baryonic mass $M_{b,in}$. In fact, if two clusters have the same values of $M_{b,in}$, but different M_{vir} , the one having smaller value of M_{vir} would have a flatter profile, since the role of the central baryonic component is larger. This was also noticed by Schmidt & Allen (2007) (Fig. 4), in the case of MS2137.3-2353, which is one of the least massive clusters in the sample that they used. They showed that increasing the values of the central stellar mass produces larger effects on the inner slope value, with respect to other cluster, because, as reported, the total mass of MS2137.3-2353 is smaller than the other sample components.

The other quantity of fundamental importance in shaping the density profiles is the random angular momentum. We have seen that a good fit to the mass/density profile of the studied clusters implies different values of j . Fig. 2 clearly shows that cluster mass and baryonic fraction are not the only fundamental parameters in building up the cluster structure. Random angular momentum, j , strongly influences cluster formation. During the collapse, particle follows orbits connected to the value of j that they have, and particles endowed with larger kinetic energy will transfer more energy (through dynamical friction) to DM with the results that DM will expand reducing the inner density. So, as previously reported, galaxies orbital parameters, and dynamics have a fundamental role in density profile formation, even larger than the baryonic content.

4.2 Problems for the Λ CDM

In the previous subsection, as in the introduction, we pointed out that Λ CDM model is unable to explain the flat density profiles observed in dwarf galaxies, and to describe the density profile of some clusters, having too flat inner slopes with respect to the Λ CDM model predictions. However this problem does not necessarily imply a problem for CDM model (e.g. DP09; Governato et al. 2010). In the clusters that we studied, only RX J1133 is in agreement with Λ CDM model predictions, while the inner slope of the density profiles of A611 and A383 contradicts the N-body simulations results. Although more recent simulations (e.g. Navarro et al. 2010) found density profiles characterized by a continuous flattening of the inner slope, this does not solve the contradiction between observations and simulations, since the quoted clusters have smaller slopes than the minimum value of the slope ($\alpha = 0.8$ at 120 pc) found in high-resolution dissipationless N-body simulations (e.g., Stadel et al. 2009). The quoted discrepancy is not restricted to the clusters studied in the present paper. On the observational side, as discussed in introduction, X-ray observations (Ettori et al. 2002; Arabadjis, Bautz & Garmire 2002; Lewis, Buote &

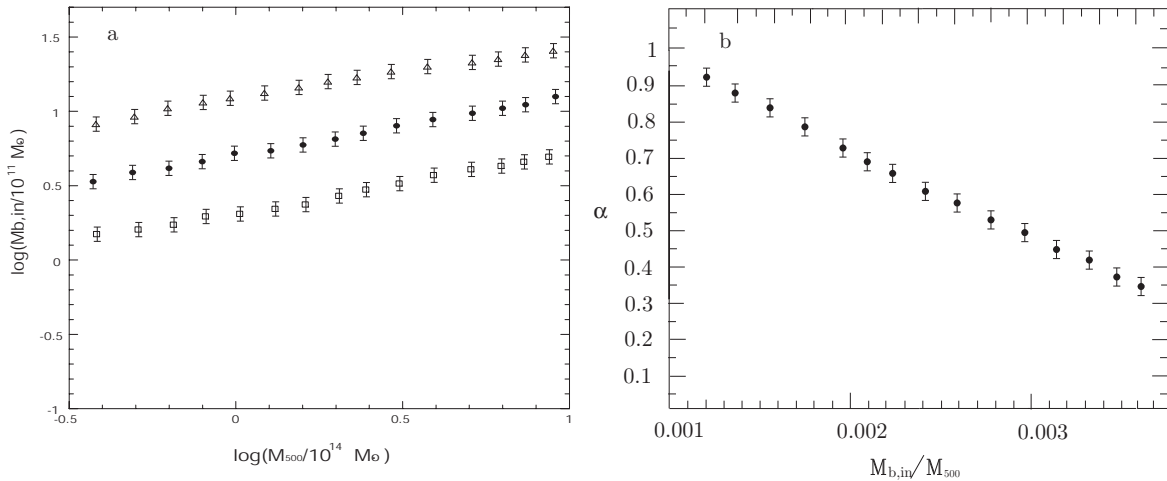


Figure 4. Fig. 4a: baryonic mass in the inner 10 kpc in terms of the total mass. Dots with 1σ error-bars, triangles with errorbars, and squares with error-bars represent the quoted relation in the cases $f_d = f_{d*}$ and $j = j_*$; $f_d = f_{d*}$ and $j = j_* \times 2$; and $f_d = f_{d*}$ and $j = j_*/2$, respectively. Fig. 4b: inner slope in terms of the ratio $M_{b, in}/M_{500}$. Dots with error-bars represent the quoted relation in the case $f_d = f_{d*}$ and $j = j_*$.

Stocke 2003), lensing (Tyson et al. 1998; Smith et al. 2001; Dahle, Hannestad & Sommer-Larsen 2003; S02; Gavazzi et al. 2003; Gavazzi 2005; S04; Bradač et al. 2008; Limousin et al. 2008), dynamics (Kelson et al. 2002; Biviano & Salucci 2006), or studies combining several techniques (e.g. S02; S04; S08; N09, N11), lead to large scatter in the value of α from one cluster to another. If some scatter can be explained, as reported in introduction by different/limited dynamic range in radius in different studies, BCG role not taken into account, or as pointed out by Morandi, Pedersen & Limousin (2010), to standard (simplified) spherical modeling of clusters, as well as the degeneracy of α with parameters like c and r_s , it is difficult to explain the large slope difference between some clusters (e.g., A611). If the scatter in the inner slope of density profile is not merely caused by limits in the techniques used, some other reason causes it. We could conclude that either some assumptions of Λ CDM model are incorrect, or given the several and noteworthy evidences supporting Λ CDM on large scales, another possibility, moreover studied in DP09, is that baryonic physics is a fundamental issue in clusters formation. Probably, as noticed in DP09, the quoted discrepancy is merely due to the fact that we are comparing two totally different systems: the one generated by dissipationless simulations, not including baryons, with real structures whose physics is not just the dissipationless physics typical of DM.

To start with, we would recall that dissipationless simulations does not include baryons, which are usually dominant in the inner part of clusters¹³, and its presence strongly influence the DM distribution. If stars form earlier than DM, baryons will compress the DM (adiabatic contraction), giving rise to steeper profiles (Blumenthal. et al. 1986; Gnedin et al. 2004; Gustafson et al. 2006). However, adiabatic contraction can be counteracted by heating of DM due to dynamical friction with cluster galaxies (El-Zant et al. 2001,

2004; Nipoti et al. 2003; Romano-Diaz et al. 2008). Several studies have tried to rescue the Λ CDM paradigm without drastic changes to the Λ CDM physics, and studying baryon physics and stellar processes in the inner parts of galaxies and clusters. Interactions of the DM with a stellar bar (Weinberg & Katz 2002; McMillan & Dehnen 2005), decay of binary black hole orbits after galaxies merge (Milosavljević & Merritt 2001), baryon energy feedback from active galactic nucleus (Peirani et al. 2008), the already quoted dynamical friction of stellar/DM clumps against the background DM halo (El-Zant et al. 2001, 2004; Romano-Diaz et al. 2008, 2009), random bulk motions of gas in primordial galaxies, driven by supernova explosions (Mashchenko et al. 2006), removal of low-angular momentum gas (Governato et al. 2010), are some of the solutions proposed. Moreover, Zappacosta et al. (2006) concluded, through X-ray observations of A2589, that processes in clusters of galaxies counteract adiabatic contraction. Infalling DM subhaloes, according to their mass, could steepen or flatten the DM cusp (Ma & Boylan-Kolchin 2004), and Nipoti et al. (2004) got similar results according to the baryon fraction of infalling galaxies.

Another important caveat is that density profiles are not universal, and that in nature may exist a distribution of inner slopes broader than that predicted by dissipationless N-body simulations. Every cluster has its own formation/merger history leading to different cluster characteristics (see Navarro et al. 2010, and S04). Several studies argue against universality of DM profiles (Jing & Suto 2000; Subramanian 2000; Ricotti 2003, 2004, 2007; Cen et al. 2004; Simon et al. 2005; Merritt et al. 2005; Graham et al. 2006; Schmidt et al. 2008; Del Popolo 2009; Ma et al. 2009; Host & Hansen 2010; Del Popolo 2012). N-body simulations as Jing & Suto (2000), Fukushige et al. (2003), Ricotti (2003), Ricotti & Wilkinson (2004) found inner slope variations from run-to-run, or with mass. Even Navarro et al. (2004, 2010) found dependence of the inner slope with mass, interpreted as a reflection of the trend between the concentration of a halo and its mass. Gao et al. (2008) in two very large cosmological simulations, found that density profiles devi-

¹³ For example, within 10 kpc, the total density distribution is dominated by the BCG in A383, RX J1133, A1201, A963, MACS 1206, MS2137-23 (S04).

ate slightly but systematically from the NFW form and are better approximated by an Einasto profile. Moreover, the shape parameter of the quoted profile changes with mass and redshift. Merrit et al. (2005, 2006) interpret the variation in profile shape with halo mass, as an indication of the fact that Λ CDM halos have not a really universal profile, as already claimed by all the authors previously quoted. By using DP09, we studied, in Del Popolo (2011), the pseudo phase-space density, arguing against universality of density profiles constituted by dark matter and baryons. From the observational point of view, Simon et al. (2005), S02, S04, S07 studies, argue against universality of density profiles.

If density profiles are not universal, is of fundamental importance to collect further high quality data, like those in A611 or A383, for larger samples of clusters (see N09, and N11) to calculate not only the mean of the distribution but also their moments. At the same time, SPH simulations, similar to that of Governato et al. (2010) for dwarfs, could be run to study clusters formation and evolution, then comparing the results with the measured distribution of inner slopes.

5 CONCLUSIONS

In the present paper we have studied how changes in random angular momentum and baryonic fraction affect density profiles of clusters with masses in the range $10^{14} - 10^{15} M_{\odot}$. The paper extends the study of DP12, on dwarf galaxies, to cluster of galaxies. A reference density profile was calculated using DP09, and then we studied how density profile changes when changing baryonic fraction and angular momentum. Similarly to the case of dwarfs, the inner density profile steepens with increasing value of the halo mass, and with decreasing values of angular momentum and baryonic fraction (see Figs. 1 and 2). This is due to the fact that when more baryons are present the energy and angular momentum transfer from baryons to DM is larger, and DM moves on larger orbits reducing the inner density. Haloes constituted only of DM have Einasto's density profiles. The previous calculation was applied to four clusters (A611, A383, MACS J1423, and RX J1133). A611 has a flat inner profile, as found by N09, and a baryonic fraction $F_b \simeq 0.15$ ($f_d \simeq 0.88$). Its density profile is re-obtained with a random angular momentum $2 \times j_*$. A383 has a flat inner profile, but steeper than that of A611. It has a similar baryonic fraction and we re-obtain its mass distribution with the typical value j_* . MACS J1423 and RX J1133 have steeper profiles, with RX J1133 well fitted by a NFW profile. They are characterized by a smaller baryonic fraction of A611 and A383, $F_b \simeq 0.1$ ($f_d \simeq 0.59$) and their profiles are re-obtained with $j = j_*/1.5$, and $j = j_*/2$, respectively. Since the baryonic content in the inner kpcs of clusters can influence their inner slope, as described by Schmidt & Allen (2007), we studied how the baryonic mass in the inner $\simeq 10$ kpc relates with the total mass of the cluster. We found a similar correlation to that found by Whiley et al. (2008), namely an increase of central baryonic mass with total cluster mass. Clusters having larger central baryonic mass have flatter profiles. We also found that a fundamental role is played by the orbital properties of the objects constituting the cluster. So, if baryon content has a certain importance in determining the final

DM distribution, the orbital parameters of galaxies, constituting the cluster, and their dynamics have a similar or even a larger importance. In summary, the density profile of clusters is strongly influenced by baryons, random angular momentum, and from the orbital parameters of galaxies, constituting the cluster, and their dynamics.

Differently from DP12, in this paper we did not study the eventual correlation of density profiles with environment. In that paper, we found that environmental effects influence density profiles of dwarf galaxies. It would be interesting to deal with this issue in a future paper, even if this study is more complicated than in the case of dwarf galaxies. This study has a fundamental complication: in order to study an eventual environment- density profile correlation, we need a large sample of clusters from which to extract isolated and unisolated clusters. From an observational point of view, there have not been many studies on the effects of the environment on the slopes of the dark matter haloes (but see DP12). Moreover, the concept of isolated or un-isolated is more or less well defined for dwarfs (e.g., Karachentsev et al. 2004, Karachentsev & Kashibadze 2006), and some samples, even if not large, are already present in literature (WHISP; Swaters et al. 2002) and in the next few years some others will be added (the LITTLE THINGS and VLA-ANGST), for the case of clusters the situation is more complicated. To our knowledge, in literature Plionis et al. (2009) identified sub-clusters within 2500 km/s of the main cluster, deliberately excluding those cluster with distorted X-ray morphology and other indications of strong interactions. Hence their sample is conservative and we would expect them to be non-interacting in a significant way with neighboring ones (even if we cannot rule out that they are weakly interacting with a structure that isn't delineated due to sub-sampling of redshifts). From that, Pimblet (2010) constructed another restricted, and more isolated sample.

Clearly, much theoretical and observational work needs to be done in order to obtain insights into the role of the environment on the density profiles of cluster of galaxies.

ACKNOWLEDGMENTS

We would like to thank Tommaso Treu, Robert Schmidt, David Sand, Alister W. Graham, Claire Lackner, Andrea Morandi, Crescenzo Tortora, Igor Karachentsev, Valentina Karachentseva, Stefano Ettori, for stimulating discussions on the topics related to the subject of this paper. Finally we thank the referee, A. B. Newman for providing constructive comments and help in improving the contents of this paper.

REFERENCES

- Aarseth S.J., Binney J., 1978, MNRAS 185, 227
- Abadi, M. G., Navarro, J. F., Fardal, M., Babul, A., & Steinmetz, M. 20010, MNRAS 407, 435-446
- Arabadjis, J. S., Bautz, M. W., Arabadjis, G. 2004, ApJ 617, 303
- Arabadjis, J. S., Bautz, M. W., Garmire, G. P. 2002, ApJ, 572, 66
- Ascasibar Y., Yepes G., Gottlober S., 2004, MNRAS, 352, 1109
- Ascasibar Y., Hoffman Y., Gottlober S., 2007, MNRAS, 376, 393
- Avila Reese V., Firmani C., Hernandez X., 1998, ApJ, 505, 37

- Avila-Reese, V., Firmani, C., Klypin, A., & Kravtsov, A. 1999, MNRAS, 310, 527
- Avila-Reese, V., Colin, P., Valenzuela, O., DOnghia, E., & Firmani, C., 2001, ApJ, 559, 516
- Bardeen J.M., Bond J.R., Kaiser N., Szalay A.S., 1986, ApJ 304, 15
- Barnes, J., & Efstathiou, G. 1987, ApJ, 319, 575
- Barrow, J.D., Silk, J., 1981, ApJ 250, 432
- Bartelmann M., Meneghetti M., 2004, A&A, 418, 413
- Bett, P., Eke, V., Frenk, C. S., Jenkins, A., Helly, J., Navarro, J., 2007, MNRAS 376, 215
- Binney J., Silk J., 1979, MNRAS 188, 273
- Blais-Ouellette S., Amram P., Carignan C., Swaters R., 2004, A&A, 420, 147
- Bonamente, et al. 2004, ApJ 614, 56-63
- Bradač, M., et al. 2005, A&A, 437, 49
- Bradač, M., et al. 2008, ApJ 681, 187
- Brough, S., Couch, W. J., Collins, C. A., Jarrett, T., Burke, D. J., & Mann, R. G. 2008, MNRAS, 385, L103
- Cardone, V. F., Piedipalumbo, E., Tortora, C., 2005A&A 429, 49
- Cardone, V. F., & Sereno, M. 2005, A&A, 438, 545 2003, ApJ, 593, 26
- Cen, R. Y., Dong, F., Bode, P., & Ostriker, J. P. 2004, arXiv:astro-ph/0403352
- Dahle H., Hannestad S., Sommer-Larsen J., 2003, ApJ, 588, L73
- Debattista, V. P., Moore, B., Quinn, T., Kazantzidis, S., Maas, R., Mayer, L., Read, J., & Stadel, J. 2008, ApJ, 681, 1076
- de Blok W. J. G., Walter F., Brinks E., Trachternach C., Oh S-H., Kennicutt R. C., 2008, AJ, 136, 2648
- de Blok, W. J. G., & Bosma, A. 2002, A&A, 385, 816
- de Blok, W. J. G., Bosma, A., & McGaugh, S. 2003, MNRAS, 340, 657
- De Lucia, G. & Blaizot, J. 2007, MNRAS, 375, 2
- de Naray R. K., McGaugh S. S., de Blok W. J. G., 2008, ApJ, 676, 920
- de Naray R. K., McGaugh S. S., Mihos J. C., 2009, ApJ, 692, 1321
- Del Popolo, A., & Gambera, M. 1996, A&A, 308, 373
- Del Popolo, A., 2009, ApJ 698, 2093
- Del Popolo, A., 2010, MNRAS 408, 1808
- Del Popolo, A., 2011, JCAP 07, 014
- Del Popolo, A., 2012, MNRAS 419, 971
- Dressler A., 1978, ApJ 243, 2
- Edge, A. C. & Stewart, G. C. 1991, MNRAS, 252, 428
- El-Zant, A. A., Hoffman, Y., Primack, J., Combes, F., & Shlosman, I. 2004, ApJ, 607, L75
- El-Zant, A. A., Shlosman, I., & Hoffman, Y. 2001, ApJ, 560, 636
- Ettori, S., Fabian, A. C., Allen, S.W., & Johnstone, R.M., 2002, MNRAS, 331, 635
- Flores, R. A., & Primack, J. R. 1994, ApJ, 427, L1
- Fukushige, T., Kawai, A., Makino, J., 2004 ApJ 606, 625-634
- Gao, L., & White, S. D. M. 2007, MNRAS, 377, 5
- Gao L., Navarro J. F., Cole S., Frenk C. S., White S. D. M., Springel V., Jenkins A., Neto A. F., 2008, MNRAS, 387, 536
- Gavazzi R., 2005, A&A, 443, 793G
- Gavazzi R., Fort B., Mellier Y., Pelló R., Dantel-Fort M., 2003, A&A, 403, 11
- Gentile, G., Salucci, P., Klein, U., Vergani, D., & Kalberla, P. 2004, MNRAS, 351, 903
- Gnedin, O. Y., Kravtsov, A. V., Klypin, A. A., & Nagai, D. 2004, ApJ, 616, 16
- Gottlöber, S. & Yepes, G., 2007, ApJ 664:117-122
- Governato, F., et al., 2010, Nature 463, 203
- Graham, A.W., Merritt, D., Moore, B., Diemand J., and Terzic, B., 2006, AJ 132, 2701
- Graham, A.W., Merritt, D., Moore, B., Diemand, J., and Terzic, B., 2006, AJ 132, 2685
- Gregory S.A., Tifft W.G., 1976, ApJ 205, 716
- Gustafsson, M., Fairbairn, M., & Sommer-Larsen, J. 2006, Phys. Rev. D, 74, 123-522
- Haarsma, D.B., et al. 2010, ApJ 713, 1037-1047
- Hayashi E. et al., 2004, MNRAS, 355, 794
- Hayashi, E., et al. 2004, MNRAS, 355, 794
- Hiotelis N., 2002, A&A, 383, 84
- Host, O., and Hansen, S.H., 2011, ApJ, 736, 52
- Hu, W., Kravtsov, A.V., 2003, ApJ 584, 702
- Hudson, M. J. & Ebeling, H. 1997, ApJ, 479, 621
- Hurley-Walker et al., 2011, arXiv: 1101.5912
- Icke V., 1973, A&A 27, 1
- Jing, Y. P., & Suto, Y. 2000, ApJ, 529, L69
- Kashlinsky, A., 1987, ApJ 312, 497
- Karachentsev I. D., Karachentseva V. E., Huchtmeier W. K., Makarov D. I., 2004, AJ, 127, 203
- Karachentsev I. D., Kashibadze O. G., 2006, Astrophysics, 49, 3
- Keeton, C. R. 2001, ApJ, 561, 46
- Kelson et al. 2002, ApJ 576, 720
- Klypin, A., Kravtsov, A. V., Bullock, J. S., & Primack, J. R. 2001, ApJ, 554, 903
- Klypin, A., Zhao, H-S., and Somerville R.S., 2002, ApJ 573, 597
- Kneib J.P., et al., 2003, ApJ, 598, 804
- Komatsu, E., Smith, K.M., Dunkley, J., Bennett, C.L., Gold, B. et al., 2011, ApJS, 192, 18
- Kowalski, M., Rubin, D., Aldering, G., Agostinho, R.J., Amadon, A. et al., 2008, ApJ, 686, 749
- Kravtsov, A. V., Klypin, A. A., Bullock, J. S., & Primack, J. R. 1998, ApJ, 502, 48
- Lackner, C. N., Ostriker, J. P., 2010, ApJ 712, 88-100
- Laporte, C. F. P., White, S. D. M., Naab, T., Ruzsokowski, M., Volker Springel, V., 2012, arXiv:1202.2357
- Le Delliou M., Henriksen R. N., 2003, A&A, 408, 27
- Lewis, A. D., Buote, D. A., Stocke, J. T., 2003, ApJ 586, 135L
- Limousin, M., et al. 2008, A&A, 489, 23
- Lin C.C., Mestel L., Shu F.H., 1965, ApJ 142, 1431
- Lin, Y.T. & Mohr, J. J. 2004, ApJ, 617, 879
- Loeb, A., Peebles, P. J. E., 2003, ApJ 589, 29
- Lukic, Z., 2009, ApJ, 692, 217228
- Ma, C.P., Chang, P. and Zhang, J., arXiv:0907.3144
- Mahdavi, A., Hoekstra, H., Babul, A., Sievers, J., Myers, S. T., & Henry, J. P. 2007, ApJ, 664, 162
- Mashchenko S., Couchman H. M. P., Wadsley J., 2006, Nat, 442, 539
- McMillan, P. J., & Dehnen, W. 2005, MNRAS, 363, 1205
- Mellier Y., 1999, ARA&A, 37, 127
- Merritt, D., Navarro, J.F., Ludlow, A., and Jenkins, A., 2005, ApJ 624, L85
- Meneghetti, M., Bartelmann, M., Jenkins, A., Frenk, C., 2007, Volume 381, Issue 1, pages 171-186
- Miller C. J., et al., 2005, AJ, 130, 968
- Milosavljevic, M., & Merritt, D. 2001, ApJ, 563, 34
- Miralda-Escudé, J. 1995, ApJ 438, 514
- Mo, H. J., Mao, S., & White, S. D. M. 1998, MNRAS, 295, 319
- Moore, B. 1994, Nature, 370, 629
- Moore, B., Governato, F., Quinn, T., Stadel, J., & Lake, G. 1998, ApJ, 499, L5
- Morandi, A., Pedersen, K., & limousin, M., 2010, ApJ 713, 491
- Navarro et al. 2010, MNRAS 402, 2134
- Navarro, J. F., et al. 2004, MNRAS, 349, 1039
- Navarro, J. F., Frenk, C. S., & White, S. D. M. 1996, ApJ, 462, 563
- Navarro, J. F., Frenk, C. S., & White, S. D. M. 1997, ApJ, 490, 493
- Newman, Andrew B.; Treu, Tommaso; Ellis, Richard S.; Sand, David J., 2011, ApJ 728, 39
- Newman, Andrew B.; Treu, Tommaso; Ellis, Richard S.; Sand, David J.; Richard, Johan; Marshall, Philip J.; Capak, Peter; Miyazaki, Satoshi, 2009, ApJ 706, 1078

- Nusser A., 2001, MNRAS, 325, 1397
- Oh, K. S. 1990, PhD thesis, Univ. California-Santa Cruz
- Oh S-H., Brook C., Governato F., Brinks E., Mayer L., de Blok W. J. G., Brooks A., Walter F., 2010, AJ 142, 24
- Padmanabhan, T., 1993, Structure formation in the universe (Cambridge: Cambridge University Press)
- Peacock J.A., Heavens A.F., 1985, MNRAS 217, 805
- Peacock, J. A., & Heavens, A. F. 1990, MNRAS, 243, 133
- Peirani, S., Kay, S., & Silk, J. 2008, A&A, 479, 123
- Percival, W.J., Reid, B.A., Eisenstein, D.J., Bahcall, N.A., Budavari, T. et al., 2010, MNRAS, 401, 2148
- Pimblett, K. A., MNRAS 411, 26372643
- Plionis, M., Tovmassian, H. M., Andernach, H., 2009, MNRAS 395, 2
- Popesso, P., Biviano, A., Böhringer, H., & Romaniello, M. 2007, A&A, 464, 451
- Power, C., Navarro, J. F., Jenkins, A., Frenk, C. S., White, S. D. M., Springel, V., Stadel, J., & Quinn, T. 2003, MNRAS, 338, 14
- Ricotti, M., and Wilkinson, M.I., 2004, MNRAS 353, 867
- Ricotti, M., 2004, MNRAS 2003, 344, 1237
- Ricotti, M., Pontzen, A., and Viel, M., 2007, ApJ 663, 53
- Ryden, B. S., 1988, ApJ 329, 589
- Rix, H.-W., de Zeeuw, P. T., Cretton, N., van der Marel, R. P., & Carollo, C. M. 1997, ApJ, 488, 702
- Romano A., et al., 2010, A&A, 514, 88
- Romano-Diaz, E., Shlosman, I., Heller, C., & Hoffman, Y. 2009, ApJ, 702, 1250
- Romano-Diaz, E., Shlosman, I., Hoffman, Y., & Heller, C. 2008, ApJ, 685, L105
- Rood H.H., Page T.L., Kintner E.C., King I.R., 1972, ApJ 175, 627
- Ryden, B. S., & Gunn, J. E. 1987, ApJ, 318, 15
- Salvador-Solé E., Solanes J.M., 1993, ApJ 417, 427
- Sand D. J., Treu T., Ellis R. S., 2002, ApJ, 574, L129
- Sand D. J., Treu T., Smith G. P., Ellis R. S., 2004, ApJ, 604, 88
- Sand, D. J., Treu, T., Ellis, R. S., Smith, G. P., Kneib, J.-P., 2008, ApJ 674, 711
- Schmidt, K.B., Hansen, S.H., and Maccio', A.V., 2008, ApJ 689, L33
- Schmidt, R. W., & Allen, S. W. 2007, MNRAS, 379, 209
- Schmidt, R. W., & Allen, S. W. 2007, MNRAS 379, 209
- Sharma, S., Steinmetz, M., 2005, ApJ 628, 21
- Schombert, J. M. 1988, ApJ, 328, 475
- Sikivie P., Tkachev I. I., Wang Y., 1997, Phys. Rev. D, 56, 1863
- Simon J. D., Bolatto A. D., Leroy A., Blitz L., 2003, ApJ, 596, 957
- Simon J. D., Bolatto A. D., Leroy A., Blitz L., Gates E. L., 2005, ApJ, 621, 757
- Smith et al. 2001, ApJ 552, 493
- Smith, G. P., Kneib, J. P., Smail, I., Mazzotta, P., Ebeling, H., & Czoske, O. 2005, MNRAS, 359, 417
- Smith, G. P., Kneib, J., Ebeling, H., Czoske, O., & Smail, I. 2001, ApJ, 552, 493
- Spanó M., Marcellin M., Amram P., Carignan C., Epinat B., Hernandez O., 2008, MNRAS, 383, 297
- Spekkens K., Giovanelli R., Haynes M. P., 2005, AJ, 129, 2119
- Spergel, D. N.; Verde, L.; Peiris, H. V.; Komatsu, E.; Nolte, M. R.; Bennett, C. L.; Halpern, M.; Hinshaw, G.; Jarosik, N.; Kogut, A.; 2003, ApJS 148, 175
- Stadel J., Potter D., Moore B., Diemand J., Madau P., Zemp M., Kuhlen M., Quilis V., 2009, MNRAS, 398, 21
- Stadel, V. J., & Quinn, T. 2003, MNRAS, 338, 14
- Subramanian, K., Cen, R., and Ostriker, J.P., 2000, ApJ 538, 528
- Swaters R. A., van Albada, T. S., van der Hulst, J. M., & Sancisi, R. 2002, A&A, 390, 829
- Swaters R. A., Madore B. F., van den Bosch F. C., Balcells M., 2003a, ApJ, 583, 732
- Swaters R. A., Verheijen M. A.W., Bershady M. A., Andersen D. R., 2003b, ApJ, 587, L19
- Tonini, C., Lapi, A., and Salucci, P., 2006, ApJ 649, 591-598
- Treu, T., & Koopmans, L. V. E. 2002, ApJ, 575, 87
- Tyson, J. A., Kochanski, G. P., & dell'Antonio, I. P., 1998, ApJ 498, L107
- Umetsu, K., & Broadhurst, T. 2008, ApJ, 684, 177
- Umetsu, K., et al. 2009, ApJ, 694, 1643
- van den Bosch F. C., Robertson B. E., Dalcanton J. J., de Blok W. J. G., 2000, AJ, 119, 1579
- Weinberg, M. D., & Katz, N. 2002, ApJ, 580, 627
- Wiley, I. M., Aragon-Salamanca, A., De Lucia, G., et al. 2008, MNRAS, 387, 1253
- White, M., 2001, A&A Volume 367, 27-32
- Williams L. L. R., Babul A., Dalcanton J. J., 2004, ApJ, 604, 18
- Yang, X., Mo, H. J., & van den Bosch, F. C. 2008, ApJ, 676, 248
- Zappacosta, L., Buote, D. A., Gastaldello, F., Humphrey, P. J., Bullock, J., Brighenti, F., & Mathews, W. 2006, ApJ, 650, 777
- Zitrin, A., et al. 2011, MNRAS DOI: 10.1111/j.1365-2966.2011.20155.x